Editorial

Living tissue intravoxel incoherent motion (IVIM) diffusion MR analysis without *b*=0 image: an example for liver fibrosis evaluation

Yì Xiáng J. Wáng

Department of Imaging and Interventional Radiology, Faculty of Medicine, The Chinese University of Hong Kong, Prince of Wales Hospital, Shatin, New Territories, Hong Kong, China

Correspondence to: Dr. Yì Xiáng J. Wáng. Department of Imaging and Interventional Radiology, Faculty of Medicine, The Chinese University of Hong Kong, Prince of Wales Hospital, Shatin, New Territories, Hong Kong, China. Email: yixiang_wang@cuhk.edu.hk.

Submitted Jan 05, 2019. Accepted for publication Jan 25, 2019.
doi: 10.21037/qims.2019.01.07
View this article at: http://dx.doi.org/10.21037/qims.2019.01.07

Intravoxel incoherent motion (IVIM) refers to the random microscopic motion that occurs in voxels on magnetic resonance (MR) images of water molecules (either intracellular or extracellular) and the microcirculation of blood. Le Bihan *et al.* (1-3) proposed the principle of IVIM which enables the quantitative parameters that separately reflect tissue diffusivity and tissue microcapillary perfusion to be estimated. Recently there has been a great interest in using IVIM technique to study diffused liver diseases such as liver fibrosis (4,5). Due to its relatively high blood supply, the liver is a very suitable organ for IVIM study. However, the liver is in the meantime particularly affected by physiological motions such as respiration and heart beating; meanwhile, the left liver is also affected by susceptibility artefact due to contents in the stomach. Although the theory of IVIM is very appealing, the practical application in the liver is difficult (5). In the case of liver fibrosis evaluation, reported results have been conflicting. Scan-rescan reproducibility can be unsatisfactory for quantification of the perfusion compartment of Dfast and perfusion fraction (PF), while Dslow may not be sensitive to pathological change (5-9).

Recently we published two small cohort studies, and the third study's report is also forthcoming. The results are better than we initially anticipated. Study-1 had 16 healthy volunteers and 33 hepatitis-b liver fibrosis patients among them 15 patients had stage-1 liver fibrosis. Study-2 had 26 healthy volunteers and 12 hepatitis-b liver fibrosis patients among them 4 patients had stage-1 liver fibrosis. All patients and healthy volunteers can be separated by IVIM analysis (10,11). Interestingly, study-2 had four patients with biopsy showing no or minimal fibrosis, and these four subjects' IVIM measurements resembled healthy volunteers (11). While our current data acquisition and analysis still remain not optimal, we believe we were able to achieve these good results by the following measures.

IVIM analysis without *b*=0 data

With most of the reported IVIM analyses, the diffusion image signal decay is computed starting from *b*=0 s/mm^2 image and then increasingly higher b-values using biexponential decay model. However, this decay process may not follow biexponential model for region of interest (ROI) based analysis. While, due to the respiratory motion and low signal-to-noise ratio, we favor ROI-based analysis for liver IVIM as opposed to voxel-wise analysis. As demonstrated in *Figures 1-3*, the signal difference between *b*=0 s/mm^2 image and *b*=1 or *b*=2 s/mm^2 images can be very substantial, the vessels (including small vessels) particularly show high signal without diffusion gradient while show dark signal when the diffusion gradient is on even at *b*=1 s/mm^2. In our two published studies we dealt with this difficulty by ignoring the *b*=0 images, and take the assumption that the remaining signal *vs. b*-value relationship follows bi-exponential decay (10,11). This simplistic approach seems worked well in our cases. In our study-2 when we tested including *b*=0 s/mm^2 image for curve fitting, there were large measurement variations among healthy subjects,

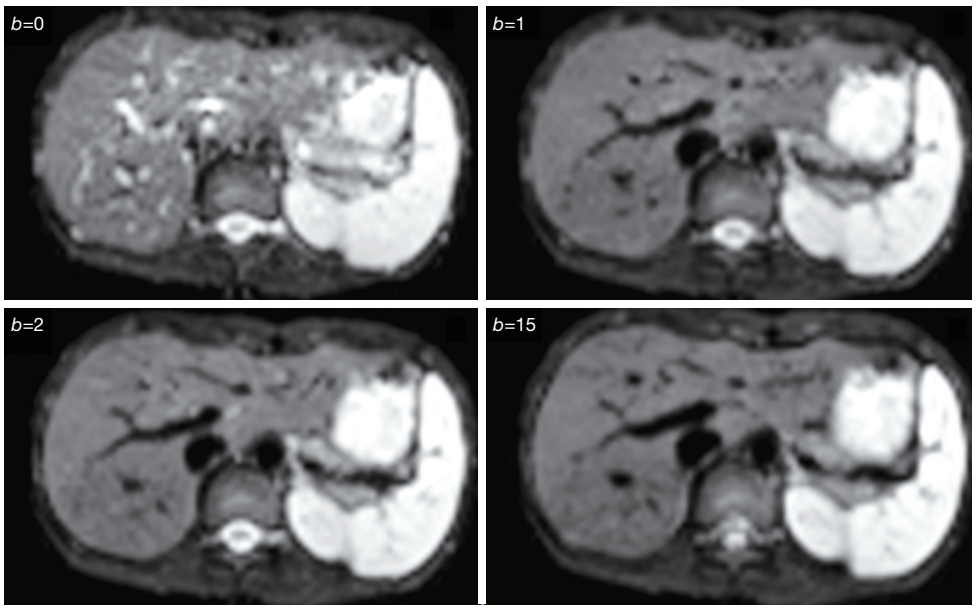

Figure 1 1.5 T liver IVIM diffusion images with *b*-value =0, 1, 2, 15 s/mm^2. The signal difference between *b*=0 s/mm^2 image and *b*=1 or 2 s/mm^2 images is dramatic, particularly the vessels show high signal without diffusion gradient while showing dark signal when the diffusion gradient is on even at *b*=1 s/mm^2. [Reproduced with permission from (11)]. IVIM, intravoxel incoherent motion.

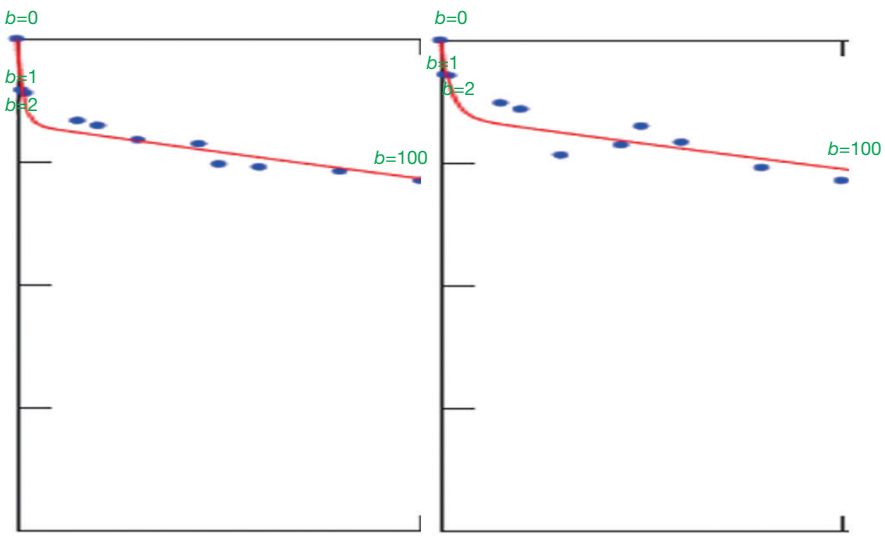

Figure 2 Two 1.5 T liver IVIM signal *vs.* *b*-value curves from *b*=0 to *b*=100 s/mm^2. Note there is a sharp decrease of signal between *b*=0 *vs.* *b*=1, while the decrease of signal between *b*=1 *vs.* *b*=2 is much smaller. Thus the curves do not follow bi-exponential decay pattern. The ROI on liver parenchyma was drawn to avoid signal contamination from large vessels well; however, inevitably some very small vessels would have been included in the ROI. IVIM, intravoxel incoherent motion; ROI, region of interest.

and patients' measurements partially overlapped with the healthy subjects' results. Thus the data of these two groups could not be separated (11). On the other hand, when we excluded *b*=0 s/mm^2 image for curve fitting, fibrosis patients' measurement and healthy subjects' measurement can be separated (11). The initially analyzed a few healthy

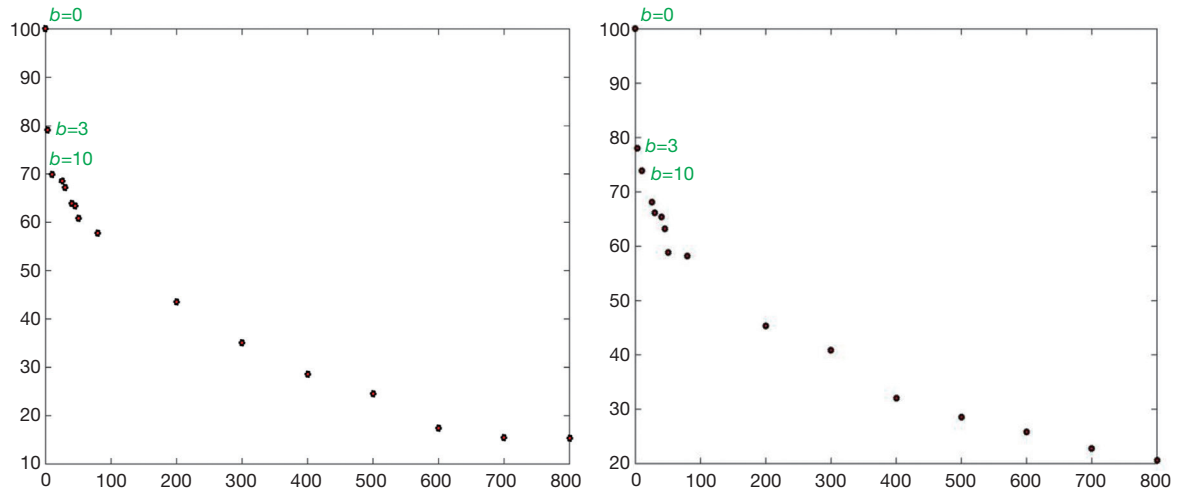

Figure 3 Two 3T liver IVIM signal *vs.* *b*-value curves from *b*=0 to *b*=800 s/mm^2. Note there is a sharp decrease of signal between *b*=0 *vs.* *b*=3, while the decrease of signal between *b*=3 *vs.* *b*=10 is much smaller. The signal decay curves between *b*=3 and *b*=800 are more likely to follow bi-exponential decay pattern. The ROI on liver parenchyma was drawn to avoid signal contamination from large vessels well; however, inevitably some very small vessels would have been included in the ROI. IVIM, intravoxel incoherent motion; ROI, region of interest.

volunteers and liver fibrosis's result from our study-3 are shown in *Figure 4*, confirming our experience.

If $SI(0)_{measure}$ is the liver signal intensity measured at *b*=0 s/mm^2, $SI(0)_{project}$ is the projected *b*=0 liver signal intensity based on bi-exponential decay model if varying *b*-value images are densely sampled and SI(0) can be therefore precisely estimated; it can be assumed that:

$SI(0)_{measure} = SI(0)_{project} + SI(0)_{ve,}$ and

$SI(b) = SI(0)_{project} \times [(1 - PF) \times \exp(-b \times D_{slow}) + PF \times \exp(-b \times D_{fast})]$, thus:

$SI(b) \times [(1 - PF) \times \exp(-b \times D_{slow}) + PF \times \exp(-b \times D_{fast})]^{-1} = SI(0)_{project} = SI(0)_{measure} - SI(0)_{ve}$

$SI(0)_{ve}$ can provide vasculature information of the living liver tissue. To precisely model the very fast initial signal decay, very dense sampling of very low *b*-value is required. In most of clinically practical cases, the sampling may be insufficient (i.e., not enough very low *b*-values). For practical approximation, this information weighted by area may be approximated by

$SI(0)_{ve/area} = [SI(0)_{measure} - SI(1)]/(\text{region of interest area})$

Alternatively, relative SI(0)ve information can also be computed by

$SI(0)ve/rel = [SI(0)measure - SI(1)]/SI(1)$

where SI(1) refers to the measured liver signal intensity when *b*=1 s/mm^2. This SI (*b*=1) can also be replaced by SI (*b*=2) or SI (*b*=3). SI (*b*=2) or SI (*b*=3) may be preferable in cases when SI (*b*=1) may contain residual high blood signal. Understandably, multiple signal averaging (NEX >1) is strongly favored for data acquisition at *b*=0 s/mm^2 and *b*=1 s/mm^2 data to improve measurement consistency of $SI(0)_{ve/area}$ and $SI(0)_{ve/rel}$.

We have preliminary analysis results of 20 healthy livers, 11 stage-1 fibrotic livers, and 5 stage-4 fibrotic livers with *b*=0 s/mm^2 and *b*=2 s/mm^2 data. The mean $SI(0)_{ve/area}$ and $SI(0)_{ve/rel}$ values were, respectively, 26.5 and 0.18 for healthy livers, 21.8 and 0.15 for stage-1 fibrotic livers, and 12.1 and 0.11 for 5 stage-4 fibrotic livers. Thus our preliminary data demonstrate a proof-of-principle that fibrotic livers have lower $SI(0)_{ve/area}$ and $SI(0)_{ve/rel}$ value compared with healthy livers; and advanced liver fibrosis is associated with even lower $SI(0)_{ve/area}$ and $SI(0)_{ve/rel}$ value.

To approximate the initial very fast decay, tri-exponential decay modeling presents another approach (12,13). However, with our current experience, the stability of tri-exponential decay modeling can be challenging at individual study subject's level.

Note that true *b*=0 s/mm^2 for IVIM diffusion imaging is actually never reachable in the presence of spoiler gradients or else gradient pulses used for magnetic resonance imaging (MRI) spatial encoding, gradient amplifier instabilities may also lead to low *b*-values less reliable (14).

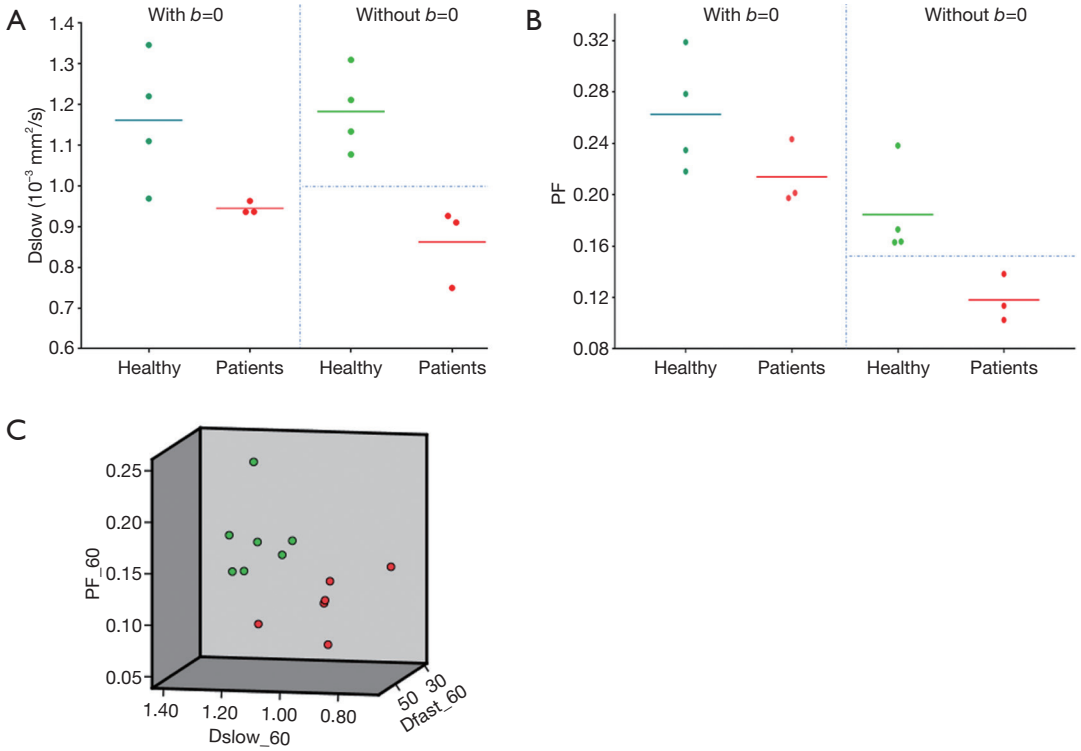

Figure 4 Preliminary results of the initially analyzed subjects from our third study. *B*-values distribution: 0, 2, 5, 10, 15, 20, 25, 30, 40, 60, 80, 100, 150, 200, 400, 600 s/mm^2, and threshold *b*-value is 60 s/mm^2, 3T scanner. (A) Four healthy volunteers and three liver fibrosis patients cannot be separated by Dslow when *b*=0 image was included for bi-exponential IVIM analysis; while the volunteers and three liver fibrosis patients can be separated by Dslow when *b*=0 image was not included for bi-exponential decay IVIM analysis; (B) the same study subjects as in (A), healthy volunteers and liver fibrosis patients cannot be separated by PF when *b*=0 image was included for analysis; while volunteers and three liver fibrosis patients can be separated by PF when *b*=0 image was not included for analysis; (C) for without b=0 image analysis, seven healthy volunteers (green dots) and six liver fibrosis patients (red dots) can be separated by 3D display of three IVIM parameters (PF, Dfast, Dslow). IVIM, intravoxel incoherent motion; PF, perfusion fraction.

Carefully select *b* value distribution and the threshold *b*-value

For liver IVIM analysis, to have sufficient and appropriate *b*-value distribution is important (5,15-17), and recently we used number of *b*-values of ~15. Generally, more *b*-values will improve fitting stability, so at this stage we would recommend acquiring as many *b*-values as practical. With current MRI technology, multiple slices covering the whole liver can be obtained with respiration-gating and 15 *b*-values in approximately 5 min.

For segmented fitting, selecting the right threshold *b*-value is more important than we initially thought (11,18). For detecting liver fibrosis, we have empirically demonstrated that threshold *b*=60 s/mm^2 works better than threshold *b*=200 s/mm^2 (9,11). It has been shown that PF offers best value in separating healthy liver *vs.* fibrotic livers, Dslow is generally not sensitive and Dfast tends to be unstable and difficult to be fitted precisely. For segmented fitting, choosing lower threshold *b*-value allows more data points to fit Dslow and therefore to fit PF and thus increases fitting reproducibility for PF (19). In addition, lower threshold *b*-value allows more perfusion component to be included in the Dslow calculation, and thus would increase the sensitivity of Dslow to liver pathologies.

Discard poor image quality files

We discard liver IVIM image series with substantial respiratory motions and poorly fitted curves (11,19). Examples of discarded scans and poorly fitted curves due to respiratory motions can be seen in our previous

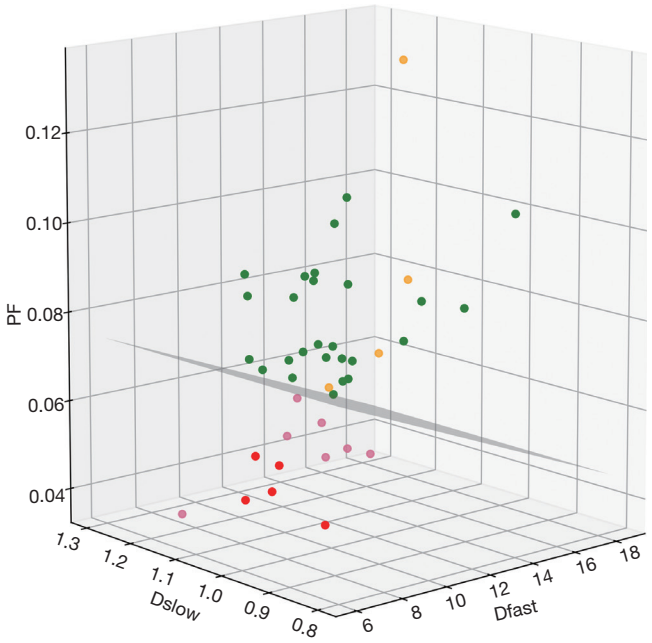

Figure 5 Study-2 results. 3D display of healthy volunteer group (green dots, n=26), patients without liver fibrosis (yellow dots, n=4), liver fibrosis stage 1–2 patient group (pink dots, n=7), and liver fibrosis stage 3–4 patient group (red dots, n=5). The volunteer group and liver fibrosis patient group can be separated by a defined plane. Note the distribution of patients without liver fibrosis (yellow dots) resembles healthy volunteers. [Reproduced with permission from (11)].

publication (11,19), and we plan to publish more examples. In our recent report (11), all 26 volunteers' images were usable, while three of 19's patients' images were un-usable. Currently, these procedures to discard image series with substantial respiratory motions and poorly fitted curves are still based on subjective adjustment and experience. Standardized and automated procedures can be developed in the future. Further, our work-in-progress suggests better image processing may allow initially un-usable IVIM data to be usable.

Incorporating all IVIM parameters for differentiation

It has noted that while PF and Dfast are correlated, these two parameters are not directly in linear proportion to each other. The perfusion compartment (PF and Dfast) and diffusion compartment (Dslow) are not significantly correlated (11). For some cases, separation of healthy volunteers and fibrotic livers are only possible when all three parameters are taken into consideration (10). Though separation of healthy livers and fibrotic livers can also be achieved by statistical means such as classification and regression tree (CART) analysis (10), we expect the 3D visualization tool we used can be convenient in practice (*Figure 5*). If the data acquisition and post-processing method are standardized, then the normal liver's data will occupy a space cluster, and if a new data entry falls out of this normal value cluster, pathology is suspected. Although we used a flat plane to separate patients and healthy volunteers (10,11), it should be noted that healthy livers and fibrotic livers do not have to be separated by a flat plane.

Other considerations

A number of measures should be considered to achieve good IVIM results. Subject (patient)'s cooperation for scanning is important to obtain high quality data for analysis. They should be well trained to maintain a shallow and regular breathing during MRI data acquisition. The balloon for respiratory-triggering should be placed on the upper abdomen where the respiratory motion is most visually evident. The more the radiographer gains experience in acquiring liver IVIM images, the more likely good quality images will be obtained. A trained radiographer may do an on-the-spot checking of image quality, and re-scan the patient if the initial IVIM image data is not of sufficient quality. As the respiratory liver displacement is more on the z-axis direction (head to foot direction) rather than in transverse plane (X-Y axis plane), some authors suggested that to scan the liver in the coronal plane may decrease the amount of motion artefact (20). Since respiration motion may be the most significant source of measurement imprecision, IVIM can also be acquired with a single-breathhold (*Figure 6*). This single-breathhold approach may have important potential, its validation in patients should be considered. As post-meal and fasted status may influence blood flow to the liver, it can be recommended that patients fast for 6 hours before liver IVIM imaging (21,22).

Drawing ROI should be careful so to avoid signal contamination from large vessels, liver border, and other artefacts. The consistency of ROI drawing also should be a research topic to be further addressed.

Finally, it can be envisaged that the thinking described here can also be applied for IVIM diffusion analysis of other pathologies and other organs, and will be particularly applicable for perfusion-rich tissues. Theoretically, the

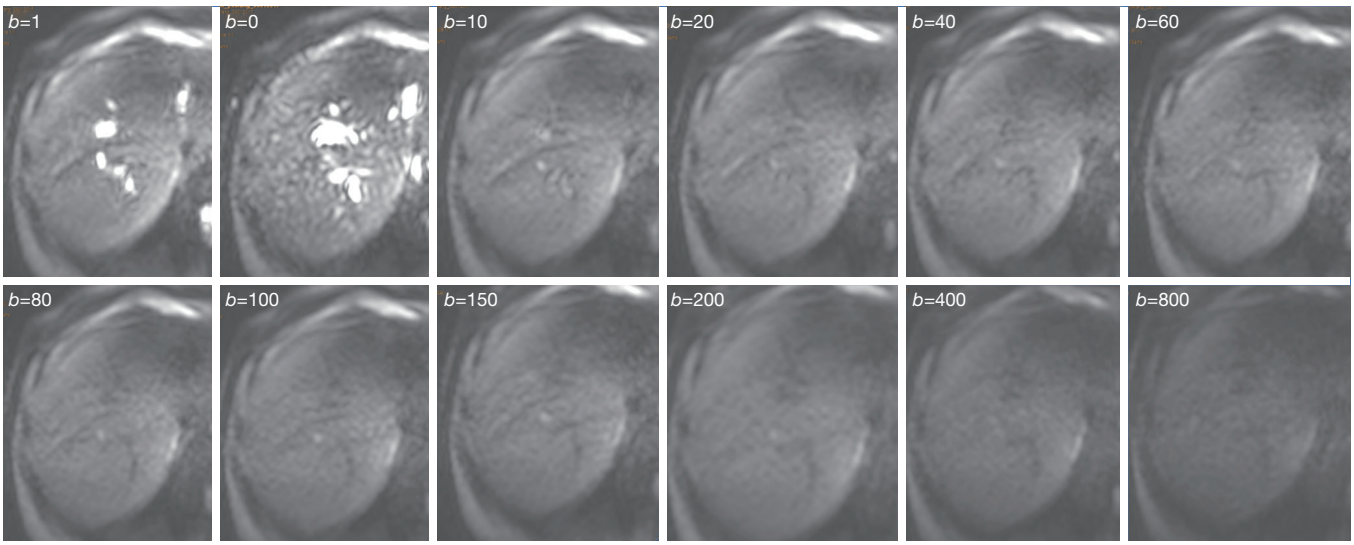

Figure 6 A single-slice single-breathhold (14 seconds) liver 12 *b*-values IVIM diffusion imaging obtained at a 3 Tesla MRI scanner equipped with dual transmitter (Achieva TX, Philips Healthcare, Best, The Netherlands). IVIM, intravoxel incoherent motion; MRI, magnetic resonance imaging.

thinking described here can also be relevant for mono-exponential decay model ADC (apparent diffusion coefficient) computing.

Acknowledgements

I thank our colleagues, collaborators, and research students who have worked, or are working with us for liver IVIM diffusion analysis. Particularly, I thank Dr. Jing Yuan, currently at Hong Kong Sanatorium & Hospital, who initiated our first liver IVIM study at the Third People's Hospital of Shenzhen, China; Dr. Olivier Chevallier of Université de Bourgogne, Dijon, France, for experimenting with us on IVIM tri-exponential decay analysis and single breathhold IVIM data acquisition. I also thank Professor Peter C. M. Van Zijl of Johns Hopkins University, USA, for discussion of the appropriateness of not including *b*=0 image for IVIM analysis.

Footnote

Conflicts of Interest: The author has no conflicts of interest to declare.

References

1. Le Bihan D, Breton E, Lallemand D, Grenier P, Cabanis E, Laval-Jeantet M. MR imaging of intravoxel incoherent motions: application to diffusion and perfusion in neurologic disorders. Radiology 1986;161:401-7.
2. Le Bihan D, Breton E, Lallemand D, Aubin ML, Vignaud J, Laval-Jeantet M. Separation of diffusion and perfusion in intravoxel incoherent motion MR imaging. Radiology 1988;168:497-505.
3. Le Bihan D, Turner R, Moonen CT, Pekar J. Imaging of Diffusion and Microcirculation with Gradient Sensitization: Design, Strategy, and Significance. J Magn Reson Imaging 1991;1:7-28.
4. Yamada I, Aung W, Himeno Y, Nakagawa T, Shibuya H. Diffusion coefficients in abdominal organs and hepatic lesions: evaluation with intravoxel incoherent motion echo-planar MR imaging. Radiology 1999;210:617-23.
5. Li YT, Cercueil JP, Yuan J, Chen W, Loffroy R, Wáng YX. Liver intravoxel incoherent motion (IVIM) magnetic resonance imaging: a comprehensive review of published data on normal values and applications for fibrosis and tumor evaluation. Quant Imaging Med Surg 2017;7:59-78.
6. Luciani A, Vignaud A, Cavet M, Nhieu JT, Mallat A, Ruel L, Laurent A, Deux JF, Brugieres P, Rahmouni A. Liver cirrhosis: intravoxel incoherent motion MR imaging--pilot study. Radiology 2008;249:891-9.
7. Guiu B, Petit JM, Capitan V, Aho S, Masson D, Lefevre PH, Favelier S, Loffroy R, Vergès B, Hillon P, Krausé D, Cercueil JP. Intravoxel incoherent motion diffusion-

weighted imaging in nonalcoholic fatty liver disease: a 3.0-T MR study. Radiology 2012;265:96-103
8. Andreou A, Koh DM, Collins DJ, Blackledge M, Wallace T, Leach MO, Orton MR. Measurement reproducibility of perfusion fraction and pseudodiffusion coefficient derived by intravoxel incoherent motion diffusion-weighted MR imaging in normal liver and metastases. Eur Radiol 2013;23:428-34.
9. Wáng YX, Li YT, Chevallier O, Huang H, Leung JC, Chen W, Lu PX. Dependence of intravoxel incoherent motion diffusion MR threshold b-value selection for separating perfusion and diffusion compartments and liver fibrosis diagnostic performance. Acta Radiol 2019;60:3-12.
10. Wáng YX, Deng M, Li YT, Huang H, Leung JCS, Chen W, Lu PX. A Combined Use of Intravoxel Incoherent Motion MRI Parameters Can Differentiate Early-Stage Hepatitis-b Fibrotic Livers from Healthy Livers. SLAS Technol 2018;23:259-68.
11. Huang H, Che-Nordin N, Wang LF, Xiao BH, Chevallier O, Yun YX, Guo SW, Wáng YX. High performance of intravoxel incoherent motion diffusion MRI in detecting viral hepatitis-b induced liver fibrosis. Ann Transl Med 2019;7:39.
12. Cercueil JP, Petit JM, Nougaret S, Soyer P, Fohlen A, Pierredon-Foulongne MA, Schembri V, Delhom E, Schmidt S, Denys A, Aho S, Guiu B. Intravoxel incoherent motion diffusion-weighted imaging in the liver: comparison of mono-, bi- and tri-exponential modelling at 3.0-T. Eur Radiol 2015;25:1541-50.
13. Chevallier O, Zhou N, Cercueil JP, He J, Loffroy R, Wáng YX. Comparison of tri-exponential decay vs. bi-exponential decay and full fitting vs. segmented fitting for modeling liver intravoxel incoherent motion diffusion MRI. bioRxiv 2018. Available online: http://dx.doi.org/10.1101/429977
14. Le Bihan D. What can we see with IVIM MRI? Neuroimage 2017. [Epub ahead of print]. doi: 10.1016/j.neuroimage.2017.12.062.
15. Lemke A, Stieltjes B, Schad LR, Laun FB. Toward an optimal distribution of b values for intravoxel incoherent motion imaging. Magn Reson Imaging 2011;29:766-76.
16. Dyvorne H, Jajamovich G, Kakite S, Kuehn B, Taouli B. Intravoxel incoherent motion diffusion imaging of the liver: optimal b-value subsampling and impact on parameter precision and reproducibility. Eur J Radiol 2014;83:2109-13.
17. ter Voert EE, Delso G, Porto M, Huellner M, Veit-Haibach P. Intravoxel Incoherent Motion Protocol Evaluation and Data Quality in Normal and Malignant Liver Tissue and Comparison to the Literature. Invest Radiol 2016;51:90-9.
18. Wurnig MC, Donati OF, Ulbrich E, Filli L, Kenkel D, Thoeny HC, Boss A. Systematic analysis of the intravoxel incoherent motion threshold separating perfusion and diffusion effects: Proposal of a standardized algorithm. Magn Reson Med 2015;74:1414-22.
19. Chevallier O, Zhou N, He J, Loffroy R, Wáng YX. Removal of evidential motion-contaminated and poorly fitted image data improves IVIM diffusion MRI parameter scan-rescan reproducibility. Acta Radiol 2018;59:1157-67.
20. Do RK, Rusinek H, Taouli B. Dynamic contrast-enhanced MR imaging of the liver: current status and future directions. Magn Reson Imaging Clin N Am 2009;17:339-49.
21. Regini F, Colagrande S, Mazzoni LN, Busoni S, Matteuzzi B, Santini P, Wyttenbach R. Assessment of Liver Perfusion by IntraVoxel Incoherent Motion (IVIM) Magnetic Resonance-Diffusion-Weighted Imaging: Correlation With Phase-Contrast Portal Venous Flow Measurements. J Comput Assist Tomogr 2015;39:365-72.
22. Burkart DJ, Johnson CD, Reading CC, Ehman RL. MR measurements of mesenteric venous flow: prospective evaluation in healthy volunteers and patients with suspected chronic mesenteric ischemia. Radiology 1995;194:801-6.

Cite this article as: Wáng YX. Living tissue intravoxel incoherent motion (IVIM) diffusion MR analysis without *b*=0 image: an example for liver fibrosis evaluation. Quant Imaging Med Surg 2019;9(2):127-133. doi: 10.21037/qims.2019.01.07

